Nonintrusive Ventilation System Diagnostics

Joseph W. O'Connell, Daisy H. Green, *Graduate Student Member, IEEE*, Brian T. Mills, Andrew Moeller, Stephen Kidwell, Kahyun Lee, *Member, IEEE*, Łukasz Huchel, and Steven B. Leeb, *Fellow, IEEE*

***Abstract*—Ventilation systems depend on periodic preventive maintenance. Unfortunately, mission critical systems, exposed to varying levels of particulates and other contaminants, may require unpredictable and highly variable maintenance intervals. Direct sensing for pressure drops or other condition metrics can provide prognostic indicators, but at the expense of the installation and maintenance burden of the sensors themselves. Rotor slot harmonics from motors have been observed for decades to track motor speed. This paper presents hardware instrumentation and a signal processing algorithm that can nonintrusively track the rotor slot harmonics of multiple fan motors in an aggregate electrical stream. Combined with a physics-based model of the motors under observation, this nonintrusive data can be used to track the maintenance condition of multiple fan motors on a single electrical service, minimizing the costs of installation and data analysis and reducing the total number of sensors necessary to track fan health. Results are demonstrated with experiments on-board a US Coast Guard Cutter.**

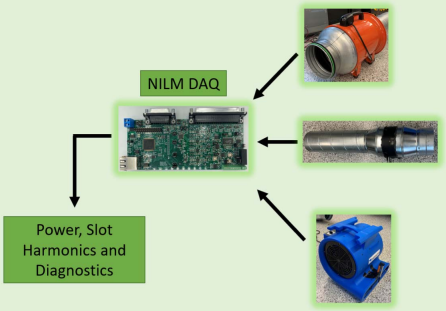

***Index Terms*—Condition monitoring, fault detection, nonintrusive monitoring, rotor slot harmonic, speed estimation.**

I. Ventilation Systems

VENTILATION systems provide fresh air and remove stagnant air for both habitable spaces and also machine processes like combustion cycles [1]–[3]. Efficient ventilation improves air quality and reduces disease transmission. Close environments require timely and effective maintenance. Degradation of airflow quantity or quality can occur for many reasons, including filter clogging, duct leakage, failed control devices like dampers or variable air volume plenums, and ingestion of foreign objects [1], [4]. Faults in ventilation systems not only degrade airflow quality, but can also lead to wasted energy. For example, the study in [5] found that 42% of the examined HVAC units had blockages or other interferences with airflow. Correcting the airflow brought 10% energy savings. Mission critical air handling systems may require sensors for pressure and flow not only for control but also for diagnostics. However, fault detection and diagnostics (FDD) techniques can be expensive due to the required number of sensors, and may still have difficulty in identifying root causes of faults [6].

Ventilation fans have performance curves that relate quantities like pressure and flow. System curves relate pressure and flow for proposed ventilation duct systems. During design, these curves inform decisions for selecting components. For example, a fan's operating point can be determined by the intersection between the system curve and fan pressure curve [7]. Many fault identification and detection schemes therefore employ rule-based methods that tabulate steady-state values for pressures and temperatures that indicate faults [8], [9].

The electrical consumption of motors in an air handler can be observed and evaluated as a proxy that replaces many sensors for FDD applications. Previously explored, rotor slot harmonics from motors in air handling systems can be used to track rotor speeds [10], [11]. This paper uses custom nonintrusive power monitoring hardware to disaggregate the slot harmonics of a collection of motors powered from a common electrical service. Signal processing identifies the harmonics associated with particular machines. Speed estimates developed from the observed slot harmonics can be used, with appropriate fan models, to estimate air flow in real time and identify blockages and leaks in air handling systems. This paper demonstrates new hardware and signal processing

Manuscript received May 14, 2021; revised June 17, 2021; accepted June 18, 2021. Date of publication June 24, 2021; date of current version August 31, 2021. This work was supported in part by The Grainger Foundation, in part by the Office of Naval Research NEPTUNE Program, and in part by MathWorks. The associate editor coordinating the review of this article and approving it for publication was Prof. Ruqiang Yan. *(Corresponding author: Daisy H. Green.)*

Joseph W. O'Connell, Brian T. Mills, and Stephen Kidwell are with the United States Coast Guard, Washington, DC 20593 USA.

Daisy H. Green, Andrew Moeller, Łukasz Huckel, and Steven B. Leeb are with the Department of Electrical Engineering and Computer Science, Massachusetts Institute of Technology, Cambridge, MA 02139 USA (e-mail: dhgreen@mit.edu).

Kahyun Lee is with the Department of Electronic and Electrical Engineering, Ewha Womans University, Seoul 03760, South Korea.

Digital Object Identifier 10.1109/JSEN.2021.3092184

1558-1748 © 2021 IEEE. Personal use is permitted, but republication/redistribution requires IEEE permission.
See https://www.ieee.org/publications/rights/index.html for more information.

Authorized licensed use limited to: MIT Libraries. Downloaded on May 31,2022 at 16:12:23 UTC from IEEE Xplore. Restrictions apply.

techniques that permit a single electrical monitor to evaluate the diagnostic condition of a collection of fans on a common electrical service. Field results are presented from US Coast Guard Cutter (USCGC) MARLIN, an 87-foot patrol boat.

II. Fan Physics

A fan curve relates shaft power to volume air flow. Therefore, a fan curve can be used to characterize power consumption changes that indicate pathologies like leaks or clogs. Because fans are often driven by induction motors, rotor slot harmonics can serve as indicators of fan blade speed. Since an induction motor's torque-speed curve determines shaft power at any particular operating speed, fan speed is an effective practical metric for determining ventilation system health, and can be correlated with blockages and leaks through examination of a fan curve. In the typical slip or speed operating regime of an induction motor, power consumption and speed are monotonically correlated. That is, for a useful range of slip, the slip as revealed by slot harmonics is closely linked to power. In the typical operating range of an induction motor, low slip (high speed) operation consumes less power than high slip (lower speed) operation. Motor or fan speed can therefore be used to identify a variety of system air flow faults. This interconnection between a fan and a motor and its utility for diagnostics are examined below.

A. Mechanical Characteristics

Ventilation systems are designed to supply specific air flow volume and pressure. System losses generate a system curve which relates pressure to airflow. The intersection between the system curve and a pressure-flow curve for the fan ("fan curve") indicates an equilibrium operating point. The Air Movement and Control Association (AMCA) standard 210 describes how to generate the pressure-flow and power curves for a fan [12]. An analytical relationship links power H and air flow:

$$H = Q P_t K \tag{1}$$

where Q is the volumetric flow rate, P_t is total pressure, and K is a thermodynamic inefficiency [13]. Flow Q and pressure P_t are non-linearly related. The simplicity of Eq. (1) belies the complex theoretical and real fan behaviors. Practical fan operation is understood not only with Eq. (1) but also using fan curves. Different types of fans have characteristic power curves, whose shapes are determined by the physical process employed to generate flow [14]. Three example power curves are shown in Figure 1. There are two major categories of fans, centrifugal and axial, which are then divided further by blade type and shrouding. This paper focuses on forward centrifugal and tube-axial fans because they are common in commercial and industrial settings, including onboard USCGC MARLIN.

For different fans operating at various points along their respective fan curves, leaky ducting or filter clogs have physically different effects. The impact of these pathologies on observed performance depends on the type of fan. The fan characteristics or curves depend on the fan type, and fan shaft power does not necessarily vary monotonically with flow rate.

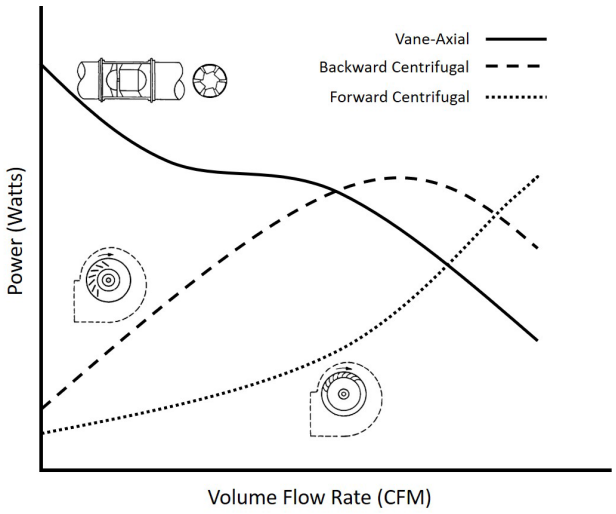

Fig. 1. Characteristic fan power curves for various fans.

TABLE I
Fault Characteristics

Fan Type	Normal Operating Point	Leaky Duct Power Impact	Clogged Filter Power Impact
Backward centrifugal	Right of power peak	Decrease	Increase
	At power peak	Decrease	Decrease
	Left of power peak	Increase	Decrease
Forward centrifugal	Any power	Increase	Decrease
Tube and vane axial	Any power (outside of stall region)	Decrease	Increase

Leaky ducts tend to increase volume flow, and clogged filters tend to impede volume flow. The effects of these pathologies on shaft power can be determined from the fan power curves. Table I summarizes expected power changes for induction motors based on the fan curves for axial and centrifugal fans under flow changes.

Axial fans move air parallel to the axis of rotation. Due to their smaller sizes and lower costs, axial fans are frequently installed in small HVAC systems. Flow analysis reveals that the pressure across the impeller of these fans is driven by the decrease in relative velocity and a rise in absolute velocity [7]. The three main types of axial fans are propeller, tubeaxial, and vaneaxial. Some axial fans have a dip in their pressure-airflow curve, indicating a stall or surge region. This region is unstable and operation in this region can lead to failure [7]. Table I assumes that the axial fan is not operating in the stall region.

Centrifugal fans operate with air entering axially through inlets on either side of the main rotating vane drum, usually either open to atmosphere or inside of a duct. Inlet air is accelerated by the blades and discharged radially. Compared to axial fans, centrifugal fans are typically more efficient and produce high static pressure, however they are also more expensive. Centrifugal fans have different fan curves based on the blade type. For forward-curved blades, air flow and power rise in lockstep, with maximum power corresponding

Authorized licensed use limited to: MIT Libraries. Downloaded on May 31,2022 at 16:12:23 UTC from IEEE Xplore. Restrictions apply.

to maximum airflow. For backward-curved blades and airfoil type centrifugal fans, the pressure curve peaks at the point of highest efficiency, with a resulting peak in the power curve.

B. Electrical Tracking

The electrical characteristics of a motor driving a fan can be measured and used as an indicator of a fan's operating point and system health. For example, for induction machine drives without speed control, slip is usually restricted to a relatively small operating range. In this range, the shaft power level varies directly with slip for most induction motors. That is, a slower induction motor shaft speed usually corresponds to a higher shaft power and vice versa. Since shaft power varies directly with slip, motor speed indicates both shaft power and therefore volume flow as indicated by the fan curve for a fan driven by the motor.

Motor speed can be determined from observed electrical waveforms by tracking slot harmonics [10]. With customized data acquisition hardware, it is possible to track the slot harmonics of several different motors on a single aggregate electrical service. That is, appropriate hardware and signal processing techniques can track multiple fans on a common electrical service.

Rotor slots in induction machines create harmonics that effect phase currents, voltages, and machine fluxes. These can be observed at frequencies:

$$f_h = f_s \left[(kR \pm n_d)\frac{1-s}{p} \pm \upsilon \right] \tag{2}$$

where f_s is the supply frequency, the non-zero integer k is the order of rotor slot harmonics, R is number of rotor slots, p is the number of pole pairs in the motor (the number of poles divided by two), the non-negative integer n_d is the order of rotor eccentricity or decentering as it rotates with respect to the stator, s is the rotor slip, and the odd integer υ is the order of stator magneto-motive force (MMF) harmonics [11], [15], [16]. Rotor slip, s, is calculated as:

$$s = \frac{n_s - n}{n_s}, \tag{3}$$

where n_s is the synchronous speed in rpm and n is the measured rotor speed. For a mechanically ideal motor ($n_d = 0$) that is fed with a pure sinusoidal supply ($\upsilon = 1$) the harmonic content in the line current demanded by the machine is expected to be distributed around the principle slot harmonic (PSH) at $k = 1$:

$$f_{psh} = f_s \left[\frac{R}{p}(1-s) \pm 1 \right]. \tag{4}$$

However, if the motor is not mechanically ideal as is generally the practical situation, there will also be harmonic content at slot harmonics frequencies for different values of n_d.

Custom data acquisition (DAQ) hardware can be used to find these harmonics in observed current waveforms even though the harmonics are small compared to the base utility frequency currents feeding the motor or motors. The custom DAQ is shown as a block diagram in Figure 2. In our experiments, six of the available eight channels sample the 3-phase voltages and currents on a shipboard 3-wire power system. Each channel samples at 8 kHz with 16-bit resolution. An additional channel is created for slot harmonic detection using an 8:1 multiplexer. The custom DAQ can simultaneously record the slot harmonic signals along with unfiltered records of the full current. The DAQ uses a zero-crossing detector for line frequency estimation. The real-time estimates of frequency are used to center or tune a switched-capacitor (SC) notch filter to eliminate utility frequency current. Because the relative amplitude of the current at the utility frequency is several orders of magnitude larger than the motor slot harmonics, the implementation of the SC filter permits the resolution of the full range of a high speed analog-to-digital converter (ADC) to measure slot harmonic currents [15]. A second-order low pass filter is applied before the SC filter as an anti-aliasing filter to restrict the bandwidth of the input signal. The cutoff frequency of the anti-aliasing filter is set to 3.1 kHz, which is much higher than the input frequency band of interest [15]. A host computer receives data from the DAQ and uses the slot harmonic stream to estimate the rotational speed of a motor's shaft. At the same time, the currents and voltages are preprocessed to compute power at an output frequency congruent with the line frequency [17]. Then, changes in electrical power consumed by a motor can be tracked. The dual streams from this nonintrusive load monitor (NILM) provide two different mechanisms for observing fan operation: electrical power and motor speed. Electrical power can be computed from the unfiltered utility frequency currents. Rotor speed can be computed from the filtered slot harmonic stream from the DAQ. Both streams, power and speed, can be used in principle to track fan health.

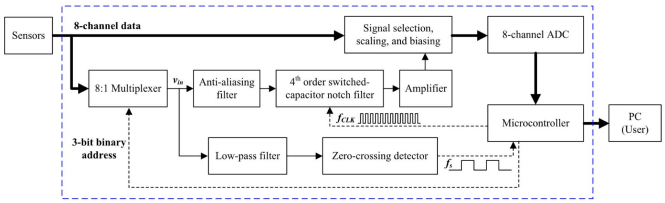

Fig. 2. Block diagram of data acquisition board [15].

The use of both streams expands the possibilities for non-intrusively monitoring a collection of fan motors on a single electrical service. Power measurements or power changes may be due to a change in fan load and a fault pathology. However, it may be difficult to associate a particular power change with a specific motor in a collection of machines. If the machines are different in other ways, for example, number of rotor bars, eccentricity, or nominal slip, then tracking slot harmonics can prove to be a valuable measurement for detecting a motor's speed uniquely in a collection of motors. The two approaches, power monitoring and speed tracking, offer some complimentary and some distinct advantages depending on the monitoring situation. The next two sections examine the utility of power monitoring and slot harmonic tracking for fan and motor fault detection.

Authorized licensed use limited to: MIT Libraries. Downloaded on May 31,2022 at 16:12:23 UTC from IEEE Xplore. Restrictions apply.

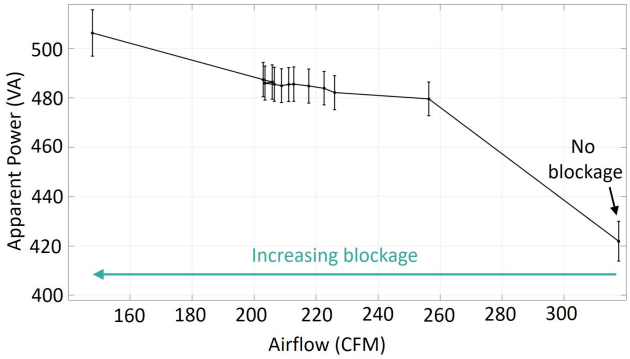

Fig. 3. Axial fan power curve.

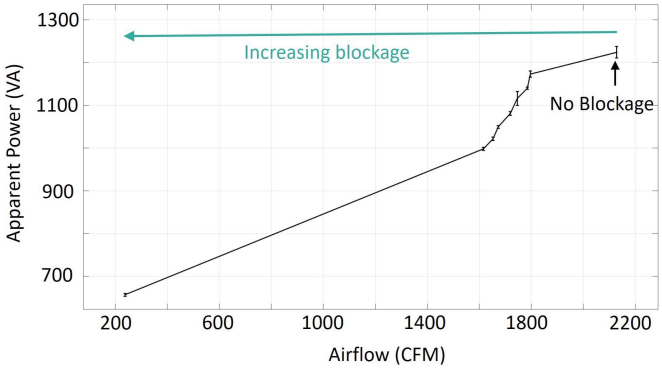

Fig. 4. Centrifugal fan power curve.

III. Fault Detection Through Power Consumption

Direct power monitoring can indicate the occurrence of diagnostic metrics for any particular installation of one or more fans. As a demonstration of the example predictions in Table I based on the example fan curves, a variety of fans were tested under different system conditions while monitoring power consumption and average air speed. All fans tested had an anemometer at their outlet to measure airflow. This section demonstrates these results and the utility of understanding fan curves and expected power changes for diagnostic and prognostic monitoring. An axial fan was tested in a duct ventilation system which introduced a system curve or loss, while a forward curved centrifugal fan was tested as a standalone air mover. To emulate blockages in the air system, filters were introduced on the intake side of the system. The filter elements consisted of varying stacks of a 1/2" polyester plastic filter, rated to Minimum Efficiency Reporting Values (MERV) 5, or 3 micron permeability. Foreign object ingestion was also emulated with complete obstruction of the fan inlets.

An SHT-30 ventilator, consisting of a tube axial fan and induction motor and was selected for its similarity in construction to the engine room exhaust and supply fans on USCGC MARLIN. After completing gradual blockage with incremental additions of up to ten filters per intake, the fan was subjected to a complete obstruction. Figure 3 shows average observed fan electrical power versus the average air speed for two minutes of fan operation. Error bars at each filter level show two standard deviations. As expected for an axial fan, power increases as airflow decreases.

A second test fan was made on a forward centrifugal fan, chosen because it closely resembles MARLIN's installed primary ventilation fan. The fan was operated for ten minutes at varying filter levels after which the fan was subjected to a complete obstruction. Figure 4 plots the average steady state power versus the average air speed at each blockage level. As expected for a forward centrifugal fan, as airflow decreases the power also decreases. It is worthwhile to note that the two standard deviation error bars on the centrifugal fan are much smaller than the axial fan, due to lower levels of turbulence.

IV. Fault Detection Using Slot Harmonic Tracking

The slip for an induction machine is monotonically related to shaft power in the typical region of operation for a healthy motor operating from a utility with fixed frequency and voltage amplitude. Shaft speed is therefore a proxy for shaft power in these situations. Observed rotor slot harmonics in the current fed to a motor indicate operating speed, and can therefore serve as an indicator of the operating state of a shaft connected fan. In situations where several motors are present on an aggregate electrical service, motors and their mechanical state can be tracked if slot harmonics can be identified that are unique to the machine of interest. Two challenges must be handled to enable nonintrusive slot harmonic tracking: compensation for variations in utility frequency and reliable identification of slot harmonics for a machine of interest in a "forest" of slot harmonics created by other machines on the utility service. Shifts in slot harmonics can be used to track changes in the mechanical fan system load, and also can be used to identify problems in the induction motor drive including broken rotor bars and other mechanical damage to the motor [18], [19]. This section presents a slot harmonic tracking algorithm applicable even when monitoring several motors. Then, experimental results are presented using an Agilent 6384B power supply. Using this controlled ac power supply permitted flexible experimentation with utility frequency variations.

A. Speed Estimation

The PSH frequency moves in a band limited by the minimum and maximum operating values for motor slip. For larger, efficient induction motors, slip is typically within a practical range of 5 to 10 percent [15]. Lower power machines, particularly in a fan application with plenty of air flow, may tolerate larger operating slips. Prior knowledge of the slip operating range is helpful to characterize an appropriate frequency window for hunting for relevant slot harmonics [16]. Various methods for rotor slot harmonic based speed estimation are reviewed in [20]. These include a frequency demodulation method [21], a maximum covariance method [22], and a short time least square Prony's method [23]. However, all of these methods only consider a single induction machine, and are not applied in a multi-machine environment.

The DAQ developed for this work rejects large utility frequency components of current and permits the full resolution of an ADC fed by a high-gain amplifier to search for slot harmonic currents. A fast Fourier transform (FFT) analysis of observed electrical currents can be used to search for slot harmonics. However, because the resolution of the frequency

Authorized licensed use limited to: MIT Libraries. Downloaded on May 31,2022 at 16:12:23 UTC from IEEE Xplore. Restrictions apply.

discrimination and resulting speed estimation depends on the size of the FFT bins, the accuracy of frequency estimation grows as the length of an observation window increases. This poses a dilemma. Long recording times provided extended data records that improve FFT frequency resolution. Shorter recording times are more likely to catch a quasi-static period of fan operation when the fan speed is essentially constant and free of mechanical disturbances. The method presented in [10] and [15] provides a balance of time and frequency resolution by finding a best-fit sinusoid within the FFT magnitude spectrum of relatively short windows of observed current. This paper builds on this method for applicability in multi-machine environments.

This approach minimizes the sum of squared errors (SSE) between the FFT magnitude spectrum of a candidate sinewave and the observed FFT magnitude spectrum of the notch-filtered motor current in an observation window. Let the candidate sinewave be defined as $s(t) = \sin(2\pi f_n t)$ with frequency f_n and unity amplitude. The independent variable is the frequency f_n, which ranges from f_1 to f_2. For a frequency window of length N_f, the vector of candidate frequencies is defined as:

$$f_n = f_1 + \frac{n}{N_f}(f_2 - f_1). \tag{5}$$

Increasing N_f increases the frequency resolution for finding the best-fit sinusoid. An exhaustive search is performed over all f_n and the frequency that minimizes the SSE is the best estimate in a squared-error sense for the location of the actual observed slot harmonic, and therefore the associated rotor speed. That is, the estimated principal slot harmonic frequency $\hat{f}_{psh}$ (or more generally the slot harmonic frequency $\hat{f}_h$) is where the SSE is minimized:

$$\hat{f}_{psh} = \min_{f_n} \mathrm{SSE}(f_n). \tag{6}$$

For f_n ranging from f_1 to f_2 and corresponding frequency indices k ranging from k_1 to k_2, the SSE is defined as:

$$\mathrm{SSE}(f_n) = \sum_{k=k_1}^{k_2} |C(f_n) \cdot |X_{s,k}(f_n)| - |X_{i,k}||^2 \tag{7}$$

where $X_{i,k}$ is the FFT spectrum of the notch-filtered motor current, $X_{s,k}$ is the FFT spectrum of a unity amplitude sine wave candidate of frequency f_n, and C is a normalizing scale factor given as:

$$C(f_n) = \sqrt{\frac{\sum_k |X_{i,k}|^2}{\sum_k |X_{s,k}(f_n)|^2}}. \tag{8}$$

So far, this method has assumed that the slot harmonic of interest is the largest peak in the window. This assumption may not hold in a multi-motor environment. Because the power information from a NILM detects when each and every motor in an installation is energized, the NILM is aware of the operation of multiple motors. In this situation, a multi-peak detection algorithm is proposed that builds on the SSE method in Eqs. (5)-(8). First, the minimum SSE sinusoid with a candidate sinewave as described above is determined with frequency f_m. This is the location of the slot harmonic of the machine with the largest peak in the window. Then, for a two-machine environment, to find the location of the slot harmonic of the second machine, a candidate signal is defined as the sum of two sinusoids,

$$s(t) = A\sin(2\pi f_n t) + \sin(2\pi f_m t), \quad A \le 1, \tag{9}$$

where A is a scale factor that is less than one. The location of the slot harmonic of the second motor is defined as the frequency that minimizes the SSE, with $X_{s,k}$ from Eq. (7) and Eq. (8) being the FFT spectrum of Eq. (9). If a window contains the slot harmonics of more than two motors, this process can be repeated with candidate signals defined as the sum of three (or more) sinusoids, as necessary. This enhanced method is demonstrated in field testing in Section V.

From the estimated PSH frequency $\hat{f}_{psh}$ the rotor speed and slip can be estimated. The estimated rotor speed in rpm is:

$$\hat{\omega}_{rpm} = \frac{60}{R}\left(\hat{f}_{psh} - f_s\right). \tag{10}$$

The estimated slip is:

$$\hat{s} = 1 - \frac{p}{R}\left(\frac{\hat{f}_{psh} - f_s}{f_s}\right). \tag{11}$$

B. Speed Estimation With Filter Blockages

To demonstrate fan speed estimation using motor slot harmonics, the centrifugal fan system was observed with various filter blockages when operating from a nominal 60 Hz utility frequency. The Agilent 6384B power supply was configured for 120 V_{RMS} output and 10 A_{RMS} current limit. The motor powering the centrifugal fan is a single-phase permanent split-capacitor (PSC) motor [24], [25]. PSC motors are commonly used in residential and commercial air handling unit blowers [26]. Speed selection is implemented with a tapped armature winding method, in which the stator winding serves as an autotransformer [25]. The lowest speed operation was selected to provide the greatest slip for the machine and therefore the greatest challenge to the speed estimation window algorithm. In this low-speed setting, the line voltage is applied to the full number of turns on the motor armature, producing the lowest machine flux and operating speed. When running at "low" speed the fan operates at roughly 30% slip.

Strictly for cross-validation and initial setting of the slot harmonic search window location in frequency, the fan speed was measured with a tachometer. Using the measured rotational speed, slip was calculated using Eq. (3). Slot harmonics for different values of v from Eq. (2) differ by $2f_s$, making $2f_s$ a good window size for locating the slot harmonic of interest [10]. Because of the high slip of this machine, filter blockages have a large effect on the motor speed. For these high slip machines, a window of length $2f_s$ that is centered on the nominal slot harmonic was used to begin the slot harmonic search:

$$f_1 = f_{prev} - f_s \le f \le f_{prev} + f_s = f_2 \tag{12}$$

where f_{prev} is the frequency of the initial or last detected slot harmonic location. This adjustable window and Eqs. (5)-(8) were used to track slot harmonics on one-second

Authorized licensed use limited to: MIT Libraries. Downloaded on May 31,2022 at 16:12:23 UTC from IEEE Xplore. Restrictions apply.

TABLE II
CENTRIFUGAL FAN SPEED AT 60 Hz

	Measured		Estimated			Error
Filters	ω_{rpm}	s	$\hat{f}_{psh}$ (Hz)	$\hat{\omega}_{rpm}$	$\hat{s}$	$\frac{\omega_{rpm}}{(\%)}$
0	1196.4	0.335	1016.8	1196.0	0.336	0.03
1	1262.4	0.299	1064.3	1255.4	0.303	0.56
2	1292.6	0.281	1094.3	1292.9	0.282	0.02
3	1319.4	0.267	1115.5	1319.4	0.267	0.00
4	1351.6	0.249	1138.5	1348.1	0.251	0.26
5	1353.2	0.248	1142.3	1352.9	0.248	0.02
6	1386.6	0.230	1170.6	1388.3	0.229	0.12
7	1408.6	0.217	1186.3	1407.9	0.218	0.05

length windows with $N_f = 1200$ (0.1 Hz frequency resolution). The initial window center for the test motor was 1020 Hz, which was the approximate observed slot harmonic location. Then Eqs. (10) and (11) were used to calculate the estimated speed and slip, respectively, with results presented in Table II. The estimated speed was then compared with the measured tachometer speed for cross-validation, as shown in Table II as absolute percentage error. The estimated speed and estimated slip closely match those calculated from the measured tachometer speed, demonstrating that slot harmonics were accurately tracked and fan speed can be reasonably measured using slot harmonics. For this centrifugal fan, the fan speed increases as expected as the system experiences progressive vent blockages, and the slot harmonic approach can clearly detect diagnostic pathologies like vent blockage and duct leaks.

C. Speed Estimation With Varying Supply Frequencies

Particularly on microgrids with limited generation capacity and finite inertia, as are found in marine environments, there are potentially significant fluctuations in supply frequency. While these fluctuations may be not effect the overall operation of the microgrid, the slot harmonic Eq. (2) effectively applies a "gain" to the utility base frequency as a function of the slip and construction of the induction motor. Relatively small variations in utility base frequency will therefore shift the location of slot harmonics, and complicate efforts to track motor speed. These frequency shifts, if not accounted for can be misinterpreted as pathologies. It is therefore essential to track supply frequency and incorporate the real time utility frequency into the slot harmonic calculations.

To explore the impacts of slight variations in supply frequency, the Agilent power supply energizing the fan motor was varied from 59.5 to 60.5 Hz in 0.1 Hz steps. The NILM operating with the enhanced DAQ uses its observations of voltage to provide a running estimate of utility frequency on a cycle-to-cycle basis. This estimate is used to compensate the slot harmonic search. The slot harmonics were tracked on one-second length windows with a frequency window of length $2f_s$ centered at 1020 Hz and $N_f = 1200$ (0.1 Hz frequency resolution). Results from these experiments are shown in Table III, with measured tachometer motor speed, slip, observed PSH, estimated speed, estimated slip, and absolute percentage error of speed. The results indicate that NILM slot harmonic tracking can effectively monitor fan rotor speed at different supply frequencies. Additional information, such as power consumption and equipment status from the NILM, can also be used to evaluate if a ventilation system is degraded. Since a fan's power consumption is relatively independent of small changes in the variable supply frequency, and as demonstrated in Section III can be used to detect ventilation blockages, this information can be examined in tandem with slot harmonic shifts to determine HVAC health.

TABLE III
CENTRIFUGAL FAN SPEED WITH VARIABLE SUPPLY FREQUENCY

	Measured		Estimated			Error
f_s	ω_{rpm}	s	$\hat{f}_{psh}$ (Hz)	$\hat{\omega}_{rpm}$	$\hat{s}$	$\frac{\omega_{rpm}}{(\%)}$
59.5	1214.6	0.319	1031.2	1214.0	0.320	0.05
59.6	1212.8	0.322	1027.8	1209.8	0.323	0.25
59.7	1211.8	0.324	1027.3	1209.1	0.325	0.22
59.8	1208.6	0.326	1025.2	1206.5	0.327	0.17
59.9	1206.6	0.329	1025.2	1206.5	0.329	0.01
60.0	1205.2	0.330	1023.3	1204.1	0.331	0.09
60.1	1204.4	0.332	1022.7	1203.4	0.333	0.09
60.2	1202.0	0.334	1019.3	1199.1	0.336	0.24
60.3	1200.4	0.336	1019.8	1199.8	0.337	0.05
60.4	1199.6	0.338	1017.7	1197.1	0.340	0.21
60.5	1196.2	0.341	1015.6	1194.5	0.342	0.14

D. Multi-Motor Frequency Space Speed Estimation

Nonintrusive monitoring scenarios are likely to involve several motors operating from a single aggregate electrical service. This situation is common, for example, with microgrids on ships. Searching for slot harmonics has proven to be of great utility in distinguishing the operation of different motors on a common electrical service. To illustrate, the previously discussed centrifugal fan was operated on the same electrical service with a 3-phase axial fan and a secondary single phase centrifugal fan (bathroom fan). All three machines were powered from the Agilent ac power supply, and the observed slot harmonics were used to approximate rotor speed on all operated machines. These comparison tests were conducted at 59.5, 60.0 and 60.5 Hz to emulate the anticipated changes in supply frequency onboard a marine micro-grid.

The motors inject a family of harmonics on to the line according to the slot harmonic equations and the inevitable imbalances in the machines that excite eccentricity harmonics. For this demonstration, the three motors were tracked with harmonics intentionally chosen relatively close to one another to reflect a the potential "worst-case" scenario, in which two machines produce similar harmonics, increasing the potential for incorrect identification. With good knowledge of the machine constructions, the machines can be tracked and their operation distinguished from the background loads. This can be seen in Figure 5, which shows the harmonics of the three fans shifting in frequency from 59.5 Hz to 60.0 Hz to 60.5 Hz. In this scenario the harmonics maintain sufficient frequency separation such that no overlap occurs.

Figure 5 also shows how different types of induction machines may react differently to changes in supply frequency. The centrifugal fan slows down as supply frequency increases while the secondary centrifugal fan and 3-phase fan

Authorized licensed use limited to: MIT Libraries. Downloaded on May 31,2022 at 16:12:23 UTC from IEEE Xplore. Restrictions apply.

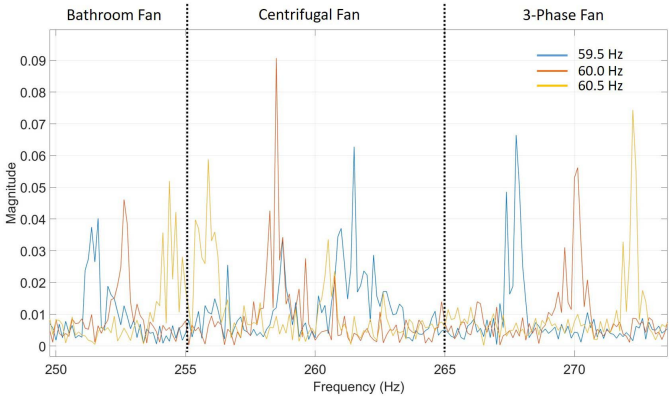

Fig. 5. Frequency space with three induction machines at various supply frequencies.

both increase speed. The centrifugal fan is powered by a single-phase capacitor run induction machine, and the shift in supply frequency alters the torque-speed curve, such that the constant torque applied by the fan blades counteracts the shift in the new endpoint. Despite variations in the supply frequency and differences in the torque-speed behaviors, the observed slot harmonics for each machine remain in distinct windows that can be reliably used to track motor operation. Specific knowledge of slot harmonic location and physical attributes of the motor can be leveraged to differentiate between harmonics, even as a power grid experiences frequency shifts or induction machines change speed due to mechanical operating conditions.

E. Rotor Bar Damage

Finally, we observe that slot harmonic information can also be used to diagnose pathologies in the motor itself, distinct from changes in the fan system. For example, rotor bar cracking [27] can occur due to thermal cycling of a motor or mechanical stress under starting [28]. It is important to distinguish gradual shifts in slot harmonics that due to a gradually leaking duct or clogging filter versus a change due to a broken rotor bar. To demonstrate the utility of slot harmonics observations in distinguishing different pathologies, two identical fans were tested, one healthy and one with a single cracked rotor bar. The tachometer-measured motor speed of the healthy motor was 1069.2 rpm, which gives a slip of 0.406. With a broken rotor bar, the expected location of the slot harmonic for the motor moves, and can be predicted by:

$$f_{brb} = f_s \left[(kR + n_d)\frac{1-s}{p} + v - 2s \right], \tag{13}$$

which indicates a predicted slot harmonic at $2f_s s$ lower than the healthy slot harmonic location [27]. Using Eq. (13) and the slip, the predicted shift in the slot harmonic is 48.7 Hz, essentially identical to the observed shift of 48.5 Hz shown in Figure 6. A nonintrusive monitor with the enhanced DAQ for tracking slot harmonics, aware of the activity of a motor from power traces, can easily detect the slot harmonic shift due to a broken rotor bar.

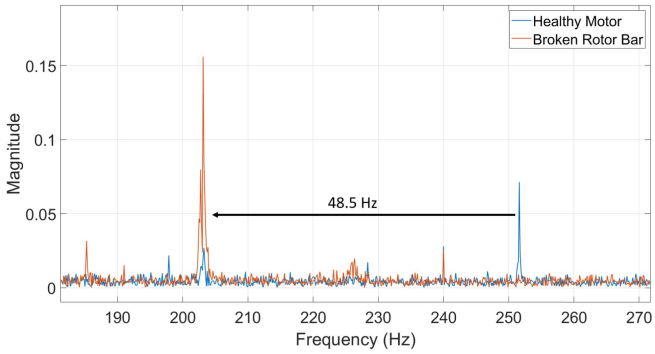

Fig. 6. Slot harmonic location shift due to rotor bar damage.

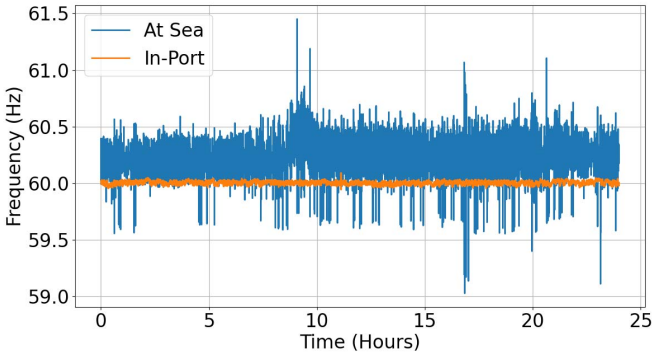

Fig. 7. Supply frequency for typical day at sea on generator power and in-port on land-based utility power.

V. Field Testing on USCGC MARLIN

This section demonstrates speed estimation and diagnostics onboard USCGC MARLIN. There are two difference scenarios in terms of frequency stability: in-port (connected to land based shore-power) and at sea (on generator power). The frequency for a typical day in-port and a typical day at sea are compared in Figure 7. In this comparison, the in-port and at sea frequencies had ranges of 0.15 Hz and 2.42 Hz, respectively.

The USCGC MARLIN has two primary ventilation systems installed, one for the engine room and the other for living spaces. Testing was conducted on the supply system for the primary habitable space. This fan system uses a belted centrifugal fan drawing air from both the weatherdeck and the internal superstructure. Speed estimation during ventilation blockage and a multi-motor environment are demonstrated while the ship is connected to shore power. Then, speed estimation is demonstrated while the ship is at sea with a changing supply frequency.

A. Primary Supply Fan

The primary supply fan employs a two-pole induction motor with 22 rotor bars rated for 3530 rpm at 60 Hz. To test the primary supply fan, filters were introduced simultaneously on both the weatherdeck "fresh" air intake and the internal re-circulation intake. Full blockage on the system, as might occur if an accidental ingestion event occurred, caused the steady-state power of the motor to drop noticeably, as expected from Table I. The motor PSH shifts as well, indicating a motor speed increase. This is similar to the observed behavior

Authorized licensed use limited to: MIT Libraries. Downloaded on May 31,2022 at 16:12:23 UTC from IEEE Xplore. Restrictions apply.

TABLE IV
MARLIN SUPPLY FAN SPEED ESTIMATES AT VARIOUS BLOCKAGE LEVELS

Blockage	$\hat{f}_{psh}$ (Hz)	$\hat{\omega}_{rpm}$	$\hat{s}$
No Blockage	1354.5	3530.46	0.0193
1 Filter	1354.5	3530.46	0.0193
2 Filters	1354.6	3530.73	0.0192
3 Filters	1354.7	3531.00	0.0192
1 Inlet Blocked	1355.6	3533.46	0.0185
2 Inlets Blocked	1358.6	3541.64	0.0162

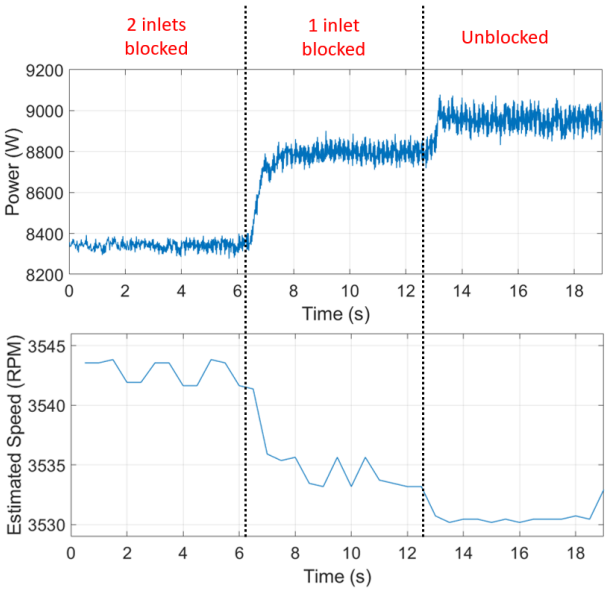

Fig. 8. Measured power and estimated speed for the supply fan with various blockage levels.

of the lab tested centrifugal fan. The SSE slot harmonic detection method in Eqs. (5)-(8) were used to nonintrusively track motor speed. Table IV shows the estimated PSH location and motor speed and slip from the slot harmonic estimation with one-second long windows and search parameters $f_1 = 1335$ Hz, $f_2 = 1375$ Hz and $N_f = 300$ (0.1 Hz frequency resolution).

Figure 8 shows the aggregate 3-phase real power stream and the estimated speed as blockages are subsequently removed. Under normal shipboard operations this supply fan is infrequently energized/secured and any clogs or leaks would happen as the fan is operating. Although the inlet blocked conditions are visible in the aggregate power stream, it would be difficult to attribute the changes in power to the supply fan when other loads are energized and consuming power. Tracking the motor PSH unambiguously identifies clogging on the ship.

B. MARLIN's Multi-Motor Environment

In addition to the primary supply fan on MARLIN, there is a hydraulic power unit (HPU) cooling fan, which draws power from the same monitored electrical grid on the ship. This cooling fan is a 3-phase axial fan, similar to the 3-phase axial fan lab-tested in Section IV. No data was acquired about the construction of the HPU cooling fan, e.g., number of rotor bars. Instead, the slot harmonics for the cooling fan were

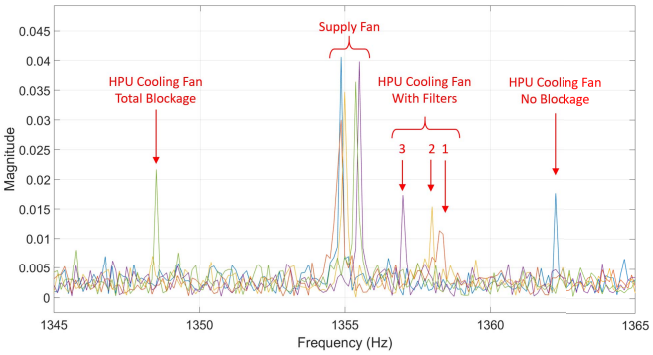

Fig. 9. MARLIN multi-motor environment.

located and tracked by running the HPU cooling fan while introducing filter blockages to slow down the fan, demonstrating that the slot harmonic tracking can be configured *ad hoc* on a field NILM. In contrast to the earlier observed centrifugal fans, this axial fan slowed down as expected as filters were introduced. This is due to an increase in torque from larger pressure differentials across the blades [7]. Up to three layers of 3 micron permeability filters were added, as well as total blockage. To "train" the NILM to recognize these slot harmonics with no other information about the machine, the HPU was energized during a period when the ship grid had other motors "off." This ability to energize, secure and physically decelerate or accelerate the fan of interest can serve as a replacement for knowledge regarding the motor's internal construction This method illustrates an important second method for identifying harmonics, when limited information is available about the machine of interest.

Once the slot harmonic window for the HPU cooling fan was identified, a multi-motor environment was tested, in which both the supply fan and HPU cooling fan were energized. The supply fan was kept at "healthy" operation, while filter blockages were introduced for the HPU cooling fan. The slow down of the HPU cooling fan as filters are introduced causes the slot harmonic to move towards the supply fan's slot harmonic. Eventually, the fully blocked axial fan's slot harmonic travels past the supply fan's harmonic location. The frequency spectrum of this multi-motor environment in various operating conditions is shown in Figure 9. In order to track the respective slot harmonics of each fan, the multi-peak detection SSE method from Eq. (9) was essential. Here, $f_1 = 1335$ Hz, $f_2 = 1375$ Hz and $N_f = 300$ (0.1 Hz frequency resolution). For Eq. (9), A is set to amplitudes ranging from 0.4 to 1 in 0.1 increments. Figure 10 shows the spectrum for a ten-second window, with the peak values. In comparison, Figure 11a shows the spectrum for a one-second window and the minimum-SSE sinusoid. These detected frequency peaks from the minimum-SSE sinusoid method match closely with the estimates from the longer ten-second window, which offered higher frequency resolution. Figure 11b shows the minimum SSE from using a single sinusoid, versus the multi-peak method with two sinusoids. These results show that even in a multi-motor environment, slot harmonics for machines of interest can be detected and tracked. Using transient detection in the NILM power stream

Authorized licensed use limited to: MIT Libraries. Downloaded on May 31,2022 at 16:12:23 UTC from IEEE Xplore. Restrictions apply.

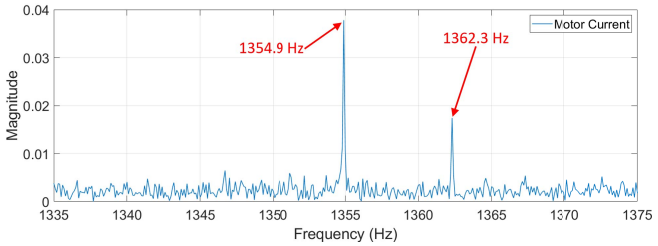

Fig. 10. Motors FFT current spectrum for a 10 second window.

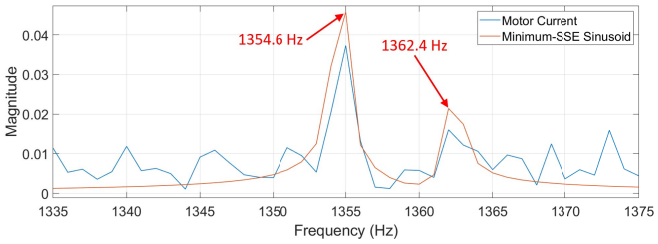

(a) FFT current spectrum for the motors and minimum-SSE sinosoids.

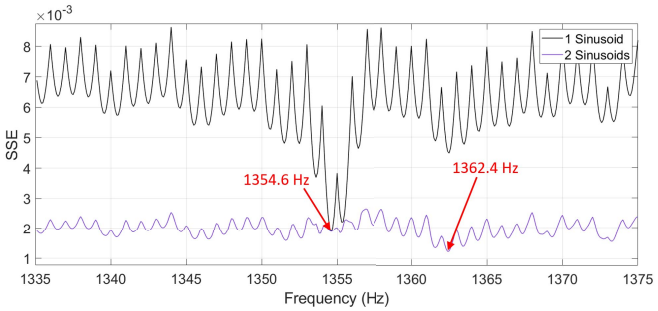

(b) SSEs according to one and two sinusoids.

Fig. 11. Current spectrum and SSEs for a 1 second window.

to determine when a load is operating can inform the slot harmonic detection algorithm as to when multi-motor slot detection is necessary.

C. MARLIN at Sea

MARLIN was observed during an underway period at sea. During this time, the installed NILM monitored supply frequency and both filtered and unfiltered current data. The supply fan was energized during the entire underway period, presenting the fan with various environmental conditions and supply frequencies. The NILM used the algorithms presented in this paper to track the supply fan slot harmonics. Supply frequency changes can impact the rotor speed as well as slot harmonic location. Figure 12 shows the estimated speed from the tracked slot harmonic as the supply frequency fluctuates from a maximum of 60.5 Hz to a minimum of 59.9 Hz, using the same method as described in Section V-A. As observed, the rotor speed decreases slightly from an estimated 3549 rpm to 3518 rpm as the ship's grid frequency decreases. Analysis of this data supports the conclusions drawn in Section IV, which indicate that slot harmonics can be tracked with a varying utility frequency when the NILM tracks utility frequency from the system voltage.

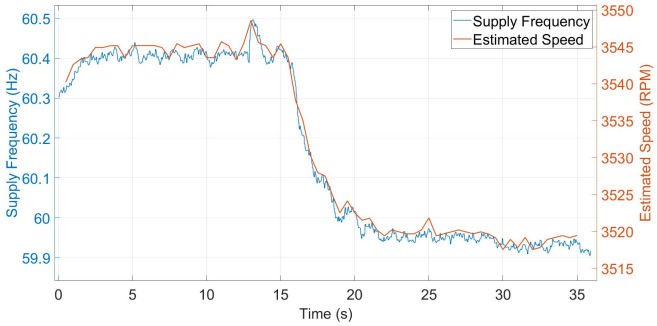

Fig. 12. MARLIN estimated speed with shifting supply frequency.

VI. Conclusion

Ventilation systems play important roles in residential, commercial, industrial, and transportation systems. They are critical energy consumers and generate substantial electrical waste when run under faulted conditions. A NILM can effectively monitor fans and their motors, providing a method or additional method for detecting and diagnosing faults. Combining knowledge of physical characteristics of installed fans with their respective electric signatures enables a NILM to track the health of an HVAC system.

The methods presented in this paper are especially valuable for aggregate monitoring of microgrids with highly-variable supply frequency. First, to demonstrate the value of power monitoring for detection of filter clogging, fans were tested using a laboratory grid as discussed in Section III. If a fan is infrequently energized and secured, clogs or leaks need to be detected while the fan is operating. Thus, slot harmonic tracking is employed to correlate specific individual fan behavior with power consumption. In Section IV, an Agilent 3-phase power supply was used to demonstrate fan speed estimation and filter clogging detection via slot harmonics. The power supply permitted demonstration of the proposed tracking and diagnostics algorithms on a utility source with flexible frequency variations. These experiments demonstrated that supply frequency needs to be tracked so that clogging or other fault conditions can be distinguished from shifts in supply frequency. A multi-machine environment was tested to demonstrate how different types of induction machines react to changes in supply frequency.

Finally, Section V demonstrated the proposed algorithms and hardware in a field microgrid on USCGC MARLIN, both in-port and at sea. The in-port experiments, which occured with a relatively stable utility frequency, demonstrated how power and slot harmonic information can be used in tandem to track ventilation health in the field. Furthermore, testing on MARLIN confirmed that these methods work well in a practical multi-machine environment served by a common electrical source. The motivation for and the applicability of the multi-peak SSE algorithm was demonstrated in this multi-machine environment. The results from MARLIN at sea confirmed that motor speed can be tracked even with a relatively highly variable supply frequency on an isolated microgrid. The laboratory and ship results together demonstrate that with a combination of equipment operation history, power consumption, and slot harmonic tracking, it is possible for

Authorized licensed use limited to: MIT Libraries. Downloaded on May 31,2022 at 16:12:23 UTC from IEEE Xplore. Restrictions apply.

a NILM system to identify fans and monitor HVAC systems for fan and motor health and speed.

ACKNOWLEDGMENT

The authors gratefully acknowledge the support and dedication of the U.S. Coast Guard and in particular the crew of USCGC MARLIN.

REFERENCES

[1] A. Singh, Y. Pandey, A. Kumar, M. K. Singh, A. Kumar, and S. C. Mukhopadhyay, "Ventilation monitoring and control system for high rise historical buildings," *IEEE Sensors J.*, vol. 17, no. 22, pp. 7533–7541, Nov. 2017.

[2] A. Verma, S. Prakash, V. Srivastava, A. Kumar, and S. C. Mukhopadhyay, "Sensing, controlling, and IoT infrastructure in smart building: A review," *IEEE Sensors J.*, vol. 19, no. 20, pp. 9036–9046, Oct. 2019.

[3] A. Kumar, A. Singh, A. Kumar, M. K. Singh, P. Mahanta, and S. C. Mukhopadhyay, "Sensing technologies for monitoring intelligent buildings: A review," *IEEE Sensors J.*, vol. 18, no. 12, pp. 4847–4860, Jun. 2018.

[4] Y. Yan, P. B. Luh, and K. R. Pattipati, "Fault diagnosis of components and sensors in HVAC air handling systems with new types of faults," *IEEE Access*, vol. 6, pp. 21682–21696, 2018.

[5] A. Cowan, "Review of recent commercial roof top unit field studies in the Pacific Northwest and California," New Buildings Inst., Washington, DC, USA, Tech. Rep., 2004.

[6] C. Laughman, "Fault detection methods for vapor-compression air conditioners using electrical measurements," Ph.D. dissertation, Dept. Archit., Massachusetts Inst. Technol., Cambridge, MA, USA, 2008.

[7] B. B. Daly and W. C. Osborne, *Wood's Practical Guide to Fan Engineering*. Colchester, U.K.: Woods Air Movement, Limited, 1978.

[8] P. Armstrong, C. Laughman, S. Leeb, and L. Norford, "Detection of rooftop cooling unit faults based on electrical measurements," *HVAC&R Res.*, vol. 12, no. 1, pp. 151–175, Jan. 2006.

[9] S. M. Namburu, M. S. Azam, J. Luo, K. Choi, and K. R. Pattipati, "Data-driven modeling, fault diagnosis and optimal sensor selection for HVAC chillers," *IEEE Trans. Autom. Sci. Eng.*, vol. 4, no. 3, pp. 469–473, Jul. 2007.

[10] U. A. Orji *et al.*, "Non-intrusive induction motor speed detection," *IET Electr. Power Appl.*, vol. 9, no. 5, pp. 388–396, Apr. 2015.

[11] S. Nandi, S. Ahmed, and H. A. Toliyat, "Detection of rotor slot and other eccentricity related harmonics in a three phase induction motor with different rotor cages," *IEEE Trans. Energy Convers.*, vol. 16, no. 3, pp. 253–260, Sep. 2001.

[12] *AMCA 210: Laboratory Methods of Testing*, A. Movement and C. Association, AMCA, Arlington Heights, IL, USA, 1999.

[13] B. Stephens, A. Novoselac, and J. Siegel, "The effects of filtration on pressure drop and energy consumption in residential HVAC systems (RP-1299)," *HVAC&R Res.*, vol. 16, no. 3, pp. 273–294, May 2010.

[14] *Industrial Ventilation, A Manual Of Recommended Practice*, A. C. Governmental Ind. Hygienists, Committee Ind. Ventilation, Washington, DC, USA, 1998.

[15] K. Lee, L. Huchel, D. H. Green, and S. B. Leeb, "Automatic power frequency rejection instrumentation for nonintrusive frequency signature tracking," *IEEE Trans. Instrum. Meas.*, vol. 70, pp. 1–11, 2021.

[16] O. Keysan and H. B. Ertan, "Real-time speed and position estimation using rotor slot harmonics," *IEEE Trans. Ind. Informat.*, vol. 9, no. 2, pp. 899–908, May 2013.

[17] J. Paris, J. S. Donnal, Z. Remscrim, S. B. Leeb, and S. R. Shaw, "The sinefit spectral envelope preprocessor," *IEEE Sensors J.*, vol. 14, no. 12, pp. 4385–4394, Dec. 2014.

[18] A. Khezzar, M. Y. Kaikaa, M. E. K. Oumaamar, M. Boucherma, and H. Razik, "On the use of slot harmonics as a potential indicator of rotor bar breakage in the induction machine," *IEEE Trans. Ind. Electron.*, vol. 56, no. 11, pp. 4592–4605, Nov. 2009.

[19] M. Drif and A. J. M. Cardoso, "Discriminating the simultaneous occurrence of three-phase induction motor rotor faults and mechanical load oscillations by the instantaneous active and reactive power media signature analyses," *IEEE Trans. Ind. Electron.*, vol. 59, no. 3, pp. 1630–1639, Mar. 2012.

[20] M. Chirindo, M. A. Khan, and P. Barendse, "Analysis of non-intrusive rotor speed estimation techniques for inverter-fed induction motors," *IEEE Trans. Energy Convers.*, vol. 36, no. 1, pp. 338–347, Mar. 2021.

[21] Z. Gao, L. Turner, R. S. Colby, and B. Leprettre, "A frequency demodulation approach to induction motor speed detection," *IEEE Trans. Ind. Appl.*, vol. 47, no. 4, pp. 1632–1642, Jul. 2011.

[22] A. Bellini, G. Franceschini, and C. Tassoni, "Monitoring of induction machines by maximum covariance method for frequency tracking," *IEEE Trans. Ind. Appl.*, vol. 42, no. 1, pp. 69–78, Jan. 2006.

[23] M. Sahraoui, A. J. M. Cardoso, K. Yahia, and A. Ghoggal, "The use of the modified Prony's method for rotor speed estimation in squirrel-cage induction motors," *IEEE Trans. Ind. Appl.*, vol. 52, no. 3, pp. 2194–2202, May 2016.

[24] H. W. Beaty and J. L. Kirtley, *Electric Motor Handbook*. New York, NY, USA: McGraw-Hill, 1998.

[25] S. J. Chapman, *Electric Machinery Fundamentals*. New York, NY, USA: McGraw-Hill, 2012.

[26] B. Stephens, "The impacts of duct design on life cycle costs of central residential heating and air-conditioning systems," *Energy Buildings*, vol. 82, pp. 563–579, Oct. 2014.

[27] A. Khezzar, M. Y. Kaikaa, and M. Boucherma, "Analytical investigation of rotor slot harmonics in a three phase induction motor with broken rotor bars," in *Proc. Eur. Conf. Power Electron. Appl.*, Sep. 2005, p. 10.

[28] G. H. Muller and C. F. Landy, "A novel method to detect broken rotor bars in squirrel cage induction motors when interbar currents are present," *IEEE Trans. Energy Convers.*, vol. 18, no. 1, pp. 71–79, Mar. 2003.

Joseph W. O'Connell received the M.S. degree in mechanical engineering from the Massachusetts Institute of Technology in 2021. He was previously stationed as an Auxiliary Division Officer aboard USCGC HEALY and an Assistant Engineer Officer onboard USCGC KIMBALL. He is currently a Lieutenant with the United States Coast Guard, stationed as a Port Engineer.

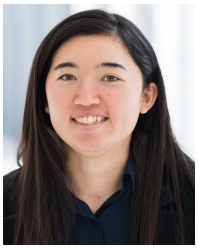

Daisy H. Green (Graduate Student Member, IEEE) received the B.S. degree in electrical engineering from the University of Hawai'i at Mānoa, Honolulu, HI, USA, in 2015, and the M.S. degree in electrical engineering from the Massachusetts Institute of Technology, Cambridge, MA, USA, in 2018, where she is currently pursuing the Ph.D. degree.

Brian T. Mills received the B.S. degree in naval architecture and marine engineering from the Webb Institute in 2016, and the M.S. degree in naval architecture and marine engineering from the Massachusetts Institute of Technology in 2021. He has served as a Student Engineer and an Assistant Engineer Officer of USCGC STRATTON (WMSL 752). He is a Lieutenant with the United States Coast Guard. He is an Assistant Engineer Officer of USCGC POLAR STAR (WAGB 10).

Andrew Moeller is currently pursuing the M.S. degree in naval architecture and marine engineering with the Massachusetts Institute of Technology. He previously served as the Damage Control Assistant on USCGC JAMES (WMSL 754) and as the Executive Officer on USCGC THUNDER BAY (WTGB 108). He is a Lieutenant with the United States Coast Guard.

Authorized licensed use limited to: MIT Libraries. Downloaded on May 31,2022 at 16:12:23 UTC from IEEE Xplore. Restrictions apply.

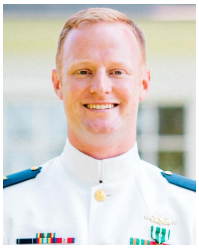

Stephen Kidwell received the M.S. degree in naval architecture and marine engineering from the Massachusetts Institute of Technology in 2020. He served as a Student Engineer and eventually an Assistant Engineer Officer onboard USCGC HAMILTON (WMSL 753) from 2015 to 2018. He is a Lieutenant with the United States Coast Guard. He is an Availability Project Manager of Coast Guard's Icebreaking, Buoy, and Construction Tender Fleet.

Kahyun Lee (Member, IEEE) received the B.S. and Ph.D. degrees in electrical engineering from Seoul National University, Seoul, South Korea, in 2013 and 2018, respectively. She was previously a Postdoctoral Associate with the Research Laboratory of Electronics, Massachusetts Institute of Technology, Cambridge, MA, USA. She is currently an Assistant Professor in Electronic and Electrical Engineering with Ewha Womans University, Seoul. Her research interests include electric machine control, signal processing, and condition monitoring.

Łukasz Huchel received the B.Sc. degree in electrical power engineering from the Silesian University of Technology, Gliwice, Poland, in 2013, the M.Sc. degree from the Department of Electrical Engineering and Computer Science (EECS), Masdar Institute of Science and Technology, Abu Dhabi, United Arab Emirates, in 2015, and the Ph.D. degree in EECS from the Massachusetts Institute of Technology, Cambridge, MA, USA, in 2021. His current research interests include the development of signal processing algorithms and hardware and software solutions for condition monitoring and diagnostics.

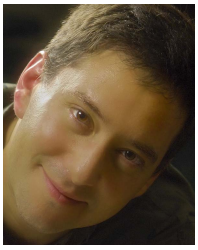

Steven B. Leeb (Fellow, IEEE) received the Ph.D. degree from the Massachusetts Institute of Technology in 1993. Since 1993, he has been a member of the Faculty of the Department of Electrical Engineering and Computer Science, MIT. He holds a joint appointment with the Department of Mechanical Engineering, MIT. He is concerned with the development of signal processing algorithms for energy and real-time control applications.

Authorized licensed use limited to: MIT Libraries. Downloaded on May 31,2022 at 16:12:23 UTC from IEEE Xplore. Restrictions apply.